Research Article Vol. 59, No. 10 / 1 April 2020 / Applied Optics 3019

applied optics

High-power, ultra-broadband supercontinuum light generated in a single-mode fiber pumped with a nanosecond passively Q-switched microchip laser

Xiaowei Huang, Zhanghao Pan, Aimin Hu, and Jun Dong*

Laboratory of Laser and Applied Photonics (LLAP), Department of Electronic Engineering, School of Electronic Science and Engineering, Xiamen University, Xiamen 361005, China
**Corresponding author: jdong@xmu.edu.cn*

Received 5 December 2019; revised 15 February 2020; accepted 23 February 2020; posted 24 February 2020 (Doc. ID 385296); published 25 March 2020

The compact, high-power, broadband continuum sources are extremely needed for developing portable instruments for various applications such as optical coherence tomography, high-resolution spectroscopy, and so on. Here, we develop a compact high-power, ultra-broadband supercontinuum (SC) light source in a single-mode fiber (SMF) pumped with a Yb : YAG/Cr^{4+} : YAG passively *Q*-switched microchip laser oscillating at 1030 nm. The spectral bandwidth of the SC light is over 1150 nm covering from 600 to 1750 nm. The maximum average output power is 181.8 mW at an input pump power of 880 mW. The optical efficiency is 20.6%, and the net conversion efficiency is as high as 51.6% with respect to the pump power coupled into the fiber. The ultra-broadband spectrum of the SC generated in the SMF is caused by the intermodal four-wave mixing (IMFWM) and cascade stimulated Raman scattering effects. Various transverse modes have been experimentally observed in SC beam generated in the SMF. Wavelength-dependent transverse modes propagating in the SMF participating in the IMFWM process dramatically expand the spectral range in the visible region. The experimental results are basically consistent with the theoretical simulations of broadband SC generated in the SMF through the IMFWM process.

https://doi.org/10.1364/AO.385296

1. INTRODUCTION

Compact supercontinuum (SC) sources with broad bandwidth have been widely used in various applications, such as optical coherence tomography (OCT) [1], molecular spectroscopy [2], and high-precision frequency measurement [3]. The femtosecond mode-locked laser-pumped photonic crystal fiber (PCF) has been extensively used in developing broadband SC sources because the dispersion of the PCF is easily designed for improving the performance of the SC source. However, high cost, complex SC sources constructed with both specially designed PCFs and mode-locked femtosecond lasers limit the applications on portable instruments and are difficult to maintain. Also, the average output power of the SC generated in the mode-locked femtosecond laser-pumped PCFs is very low, and further limit the applications of such SC sources. The pump laser system is one of the key factors to determine the compactness and cost of the SC systems. Therefore, low-cost and high peak power picosecond or nanosecond lasers are used as a potential pump laser system to produce high-power SC. However, for the picosecond or nanosecond fiber lasers, their peak power is not high enough to be used for directly generating the SC. It is necessary to enhance the peak power by using a master oscillator power amplifier (MOPA) [4]. A SC generated in the nonlinear medium pumped with a MOPA further increases the cost and complexities. The passively *Q*-switched microchip lasers (PQSMLs) with high peak power are ideal pump sources for developing a compact high-power SC. Another factor that needed to be considered is the fiber types. Although PCFs are widely used for generating SC, the input pulse energy is restricted by the low damage threshold arising from the small core size. Thus, the achievable spectral optical power density of the SC is low, and it is difficult to realize high power output. The commercial silica single-mode fibers (SMFs) are widely used in developing a high-power fiber laser because they are high quality and economical. The SMFs have been used in generating SC because they have low loss in the near-infrared region and can support higher power in the fiber core.

With the high peak power PQSMLs as the pump source, compact, economic, and broadband SC sources can be

developed in SMFs under high-intensity laser radiation. Some works using SMFs as a nonlinear medium have been published [5,6] and the broadband SC light has been generated in a SMF pumped with a Nd:YAG PQSML in the large dispersion region [7]. However, the output power of the SC is low owing to low pump power coupling into the SMF. There is a valley in the spectrum of the SC generated in the short-wavelength region. In addition, there are some physical mechanisms of generating high-performance SC is underutilized in SMFs, and the spectral bandwidths of 650 to 1000 nm [6,8–10] are needed to be further promoted.

It is well known that various nonlinear effects induced by the pulsed laser participate in the formation of the SC in optical fibers. Four-wave mixing (FWM) is one of the nonlinear effects which was first observed in optical fiber [11]. The intermodal four-wave mixing (IMFWM) induced by the Stokes, anti-Stokes, and pump light oscillating in different transverse modes has recently been widely studied. However, the IMFWM is only observed in the multi-mode fibers and few-mode fibers [12,13]. The 532 nm green light has been used to study the IMFWM in the SMF-28 laser oscillating in the visible region [14]. And the visible lasers generated in the SMF were explained with a theoretical model based on IMFWM and a new frequency was predicted, which verified that IMFWM can be achieved in the multi-mode region of single-mode fiber. However, up to now, supercontinuum generation by IMFWM has only focused on PCF or multi-mode and few-mode fibers [13,15–17]. The output powers from these fibers are low. There is no report on generation of a SC in a SMF through the IMFWM process. The physical mechanism of generating a SC through the IMFWM effect to expand the spectral range in a SMF pumped with a high peak power laser is worth investigating.

High peak power, sub-nanosecond Yb : YAG/Cr^{4+} : YAG PQSMLs oscillating at 1030 nm have been demonstrated [18,19]. Compared to a Nd:YAG PQSML, the short wavelength at 1030 nm is favorable for further increasing the coupling efficiency between different modes and providing more energy for the fiber modes coupling [20]. Therefore, by adopting a high peak power, nanosecond Yb : YAG/Cr^{4+} : YAG PQSML as a pump source, high-power, broadband SC light should be generated in a commercial standard SMF, which has potential application on developing compact portable instruments.

In this paper, we developed an ultra-broadband SC with a bandwidth of 1150 nm from 600 nm to 1750 nm in a SMF pumped with a nanosecond Yb : YAG/Cr^{4+} : YAG PQSML. The average output power of 181.8 mW was obtained at an input pump power of 880 mW. The net conversion efficiency is 51.6% with respect to the pump power coupling efficiency of 40%. The generation of ultra-broadband SC in a SMF pumped with a nanosecond PQSML was attributed to the IMFWM process.

2. EXPERIMENTAL SETUP

The experiment setup of a PQSML pumped SMF for SC generation is shown in Fig. 1. A Yb : YAG/Cr^{4+} : YAG PQSML oscillating at 1030 nm was used as the pump source. The pulse width is 1.19 ns and the repetition rate is set to 17 kHz. The maximum average output power is 880 mW and the peak power is about 43 kW. Lens pairs with focal lengths of 100 mm and 15 mm form a collimating-focusing system for coupling a spatial laser into the fiber. There is about 4.5% loss of the pump power after collimating and focusing the lens. A 105 m long SMF (SMF-28) was used as the nonlinear medium. The coupling efficiency was measured to about 40%. An attenuator settled before the fiber was used to adjust the incident pump power. The spectrum of the SC is recorded with an optical spectrum analyzer (Anritsu, MS9740A; its spectral range is from 600 to 1750 nm).

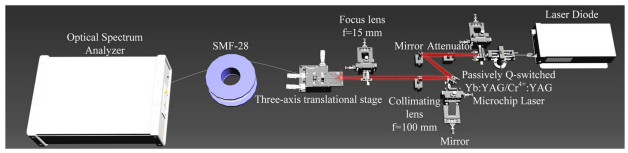

Fig. 1. Experimental setup.

3. EXPERIMENTAL RESULT AND DISCUSSION

The evolution of the spectra of the SC light generated in the SMF-28 with the input pump power is shown in Fig. 2. The input pump power from the Yb : YAG/Cr^{4+} : YAG PQSML was experimentally controlled by using an attenuator. When the input pump power of the PQSML is 2.5 mW, the corresponding peak power is about 124 W. However, the peak power in the fiber was only about 49 W because the coupling efficiency was 40%. The threshold pump power for realizing stimulated Raman scattering (SRS) in a SMF was estimated to be 68.8 W according to the expression [21] by using the parameters $g_R = 10^{-13}$, $\alpha = 1$ dB/km, and $A_{\text{eff}} = 42.8\ \mu\text{m}^2$ for the SMF. Therefore, the pump power passed through the SMF did not induce any nonlinear effects, only the pump laser at 1030 nm was observed, as shown in Fig. 2(a). The laser at 940 nm (labeled as LD) was also observed because the residual pump laser for the PQSML was coupled into the fiber. The spectral ranges from 600 to 900 nm and beyond 1030 nm are marked as noise at short wavelength and noise at long wavelength of the optical spectrum analyzer. When the input pump power of the PQSML increased to 7.8 mW (about 81 W of peak power), the Raman laser at 1079 nm oscillates, as shown in Fig. 2(b). The Raman laser oscillating at 1079 nm (marked as R_1) is attributed to the Raman conversion from the pump laser at 1030 nm with a 13.2 THz Raman frequency shift. The other two lasers (marked as AS and S) oscillate at 1004 nm and 1058 nm, respectively. The photon energies of these two lasers at 1004 nm and 1058 nm are nearly equal to 2 times of the photon energy of the pump laser at 1030 nm, which satisfies the FWM energy conservation Eq. (2) $\hbar\omega_p = \hbar\omega_{as} + \hbar\omega_s$. The lasers oscillating at 1004 nm and 1058 nm indicates that the phase-matching condition is satisfied for the FWM process with a laser at 1030 nm as the pump source. Further increasing the pump power of the PQSML up to 13.2 mW, as shown in Fig. 2(c), a second-order Raman laser at 1135 nm (marked as R_2) appears due to the cascaded SRS converted from the first-order Raman laser at 1079 nm with a frequency shift of 13.7 THz. After the input power is raised to 18.4 mW, another Raman laser at 1113 nm (marked as SR_1)

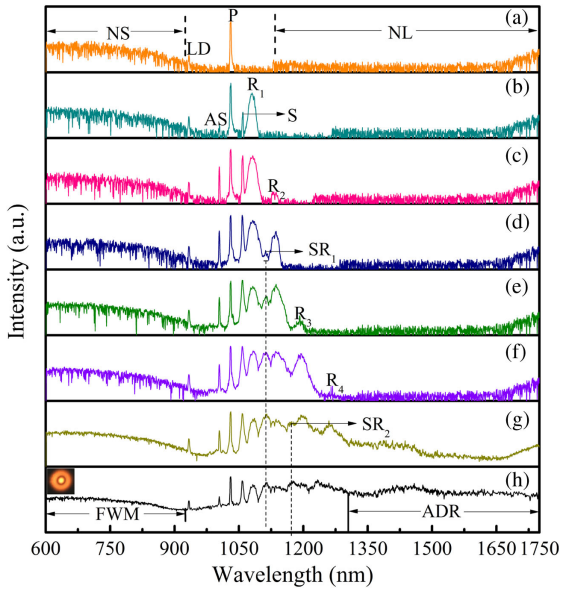

Fig. 2. Spectra of SC generated in a 105 m SMF fiber at different input pump powers (peak power). (a) $P = 2.5$ mW (124 W), (b) 7.8 mW (386 W), (c) 13.2 mW (652 W), (d) 18.4 mW (910 W), (e) 28.6 mW (1.4 kW), (f) 41.2 mW (2.04 kW), (g) 61.4 mW (3.04 kW), and (h) 122.6 mW (6.06 kW). The inset in (h) shows the far-field distribution in visible. NS, noise of the short-wavelength part; NL, noise of the long-wavelength part; ADR, anomalous dispersion regime; FWM, four-wave mixing.

oscillates, which is attributed to the Raman conversion from the Stokes laser at 1058 nm with a Raman frequency shift of 13.7 THz, as shown in Fig. 2(d). When the input pump power of the PQSML reaches 41.2 mW, the third-order and fourth-order Raman lasers at 1193 nm (R_3) and 1259 nm (R_4) are generated with the cascade SRS process with a Raman frequency shift of 13.7 THz, as shown in Figs. 2(e) and 2(f). Subsequently, when the input pump power is increased to 61.4 mW, another second-order Raman laser oscillates at 1172 nm (SR_2), as shown in Fig. 2(g), and is converted from the first-order Raman laser at 1058 nm with the cascade SRS process. The cascade SRS plays a key role in generating new lasers and further expanding the laser spectrum. In addition, the laser spectrum is expanded in the short-wavelength range covering from 600 to 900 nm, as shown in Fig. 2(g).

With the further increase of the pump power up to 122.6 mW, the spectrum of the SC expands dramatically on both blue and red sides; a spectrum covering 600 to 1750 nm was observed, as shown in Fig. 2(h). The far-field transverse profiles of the SC laser were observed in the visible region. The transverse profile obtained with a camera is distinguished as a bright orange high-order LP02 mode, as shown in the inset of Fig. 2(h), suggesting that the process of energy transfer to visible parts is related to IMFWM and the short-wave spectral range is lower than 600 nm. Therefore, dramatic expansion of the spectrum of the SC generated in the SMF is attributed to the combination effect of the IMFWM process together with other nonlinear effects such as soliton fission [22] and Raman soliton self-frequency shift (SSFS) [23,24]. Soliton fission and Raman SSFS further expand the spectrum of the SC and enhance the spectral intensity at the visible region. When a SMF is pumped in the anomalous dispersion regime, the high-order solitons generate and break up into a number of fundamental solitons. In this nonlinear process, a nonlinear mechanism, known as Cherenkov radiation, causes the soliton to transfer energy to the wavelength in the normal dispersion regime [25–28]. The laser wavelength at 1030 nm of the Yb : YAG/Cr^{4+} : YAG PQSML with high peak power is in the normal dispersion regime of the fiber, and nearly 300 nm away from the zero-dispersion wavelength (ZDW) of the fiber. This ensures that the pump light has a sufficient interaction length with the Stokes light [29]. Therefore, over 4 orders Stokes lasers through the cascade SRS process were generated in the experiment.

When the pump power is increased to the available maximum input pump power of 880 mW, the broadband SC laser covering from 600 to 1750 nm is maintained and intensities of the lasers at different wavelengths increase, as shown in Fig. 3. The bandwidth is 1150 nm, which is limited by the spectral range of the optical spectral analyzer. The maximum output power of the SC light is 181.8 mW at the input pump power of 880 mW, and the optical efficiency is 21%. The net conversion from the coupled pump power to SC light is estimated to be as high as 51.6% with a coupling efficiency of 40%. The broadband spectrum can be divided into three regions by the first-order Raman laser wavelength (R1) and ZDW, namely, cascaded IMFWM regime (I), cascaded Raman regime (II), and anomalous dispersion regime (III), respectively. In the regime (I), the laser spectrum in the visible becomes flat and intensities of the lasers at the visible region increase at high pump power level owing to the effective IMFWM processes. In the regime (II), the multiple peaks overlapping with a flat laser spectrum are caused by the cascade SRS effect. The high peak power of input pump pulses ensures the high-order Raman conversion with the cascade SRS effect. The multiple peaks appearing over the laser spectrum at the near-infrared region can be alleviated by controlling the pump pulse intensity and the length of the SMF. Therefore, the flat spectrum of the SC at the near-infrared region is expected. In the spectral regime (III), a multiple-spike laser spectrum of the SC can be alleviated by adjusting the pump power intensity for generating solitons. Cascade SRS and IMFWM play major roles for generating broadband SC light in the Yb : YAG/Cr^{4+} : YAG PQSML pumped SMF. The cascade SRS effect contributes to expansion of the SC spectrum in the infrared region and far-detuned IMFWM is responsible for the extension of the SC spectrum toward the visible [13]. Cascade SRS mainly transfers the pump light energy to the laser oscillating at the long-wavelength side. The IMFWM consumes the energy of the pump light to produce downshifted Stokes photon and upshifted anti-Stokes photon, so the laser at the short-wavelength side is mainly caused by IMFWM. Since the spectral broadening of the redshifted direction is caused by both the Stokes lasers with SRS and FWM processes, the energy generated in the redshifted direction is greater than that generated in the blueshifted direction. The power drop at 1372 nm is mainly caused by the water absorption peak of the fiber.

The transverse modes at 1030, 1004, 695, and 645 nm after passing through some narrow bandwidth filters designed at different wavelengths are measured with a beam profile analyzer. The transverse profiles of SC light generated in the SMF-28 at

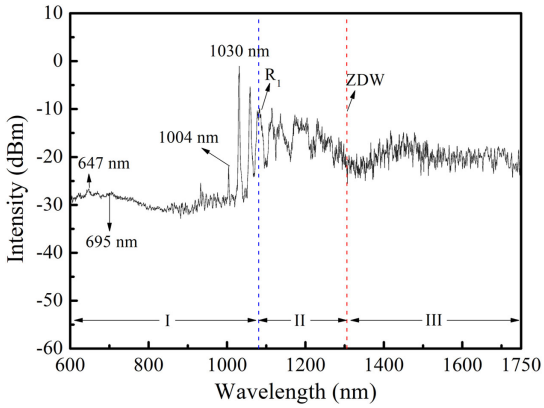

Fig. 3. Final spectra of SC generated in a 105 m SMF fiber with an input pump power of 880 mW. I: cascaded IMFWM regime, II: cascaded Raman regime, III: anomalous dispersion regime. R_1 and ZDW represent the first Raman line of pump light at 1078 nm and zero-dispersion wavelength at 1310 nm, respectively.

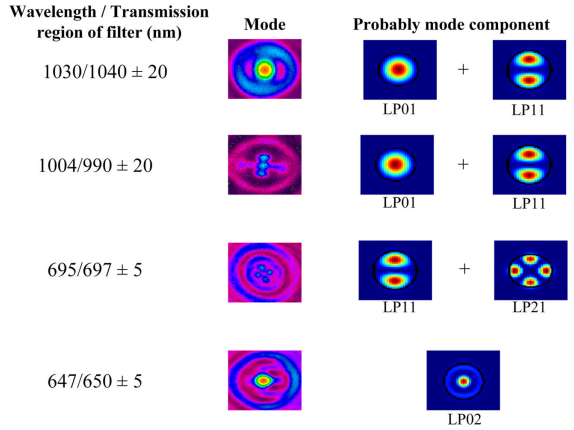

Fig. 4. Experimentally obtained transverse modes at 1030, 1004, 695, and 647 nm.

different wavelengths are shown in Fig. 4. The experimentally obtained transverse patterns at 1030 and 1004 nm are confirmed as mixed modes (LP01, LP11). The transverse pattern at 695 nm is made up of LP11, LP21, and some other modes. The transverse pattern at 647 nm is made up of LP02. The experimentally obtained transverse profiles at different wavelengths provide strong evidence for IMFWM playing key role in generating a SC with a flat spectrum in the visible region. The energy at the short-wavelength region in the SMF is fully extracted with oscillating of high-order modes through the IMFWM process. Therefore, ultra-broadband SC light covering from 600 to 1750 nm is achieved in a SMF pumped with a nanosecond Yb : YAG/Cr^{4+} : YAG PQSML.

Table 1 summarizes the performance of SC light generated in a SMF pumped with a Yb : YAG/Cr^{4+} : YAG PQSML. We compared our results with the results obtained in the multi-mode and few-mode fibers from other research groups [7,13,15]. From Table 1, we can clearly see that the bandwidth of the SC generated in the single-mode fiber pumped with a PQS microchip laser can be effectively widened with the

Table 1. Performance of SC Light Generated in the SMF, Multi-Mode, and Few-Mode Fibers Pumped with a PQS Microchip Laser

Spectral Bandwidth	Pump Power	Output Power	Optical Efficiency	Ref.
~1100 nm	51.3 mW	3.8 mW	7.4%	[7]
~1790 nm	50 mW	13 mW	26%	[13]
~1100 nm	57 mW	—	—	[15]
~1150 nm	880 mW	181.8 mW	20.6%	This work

IMFWM effect, and a high output power can be obtained under high pump power pumping. The optical efficiency can be further improved by optimizing the coupling efficiency of the pump power. Compared to the peaked spectrum in the visible region obtained in the few-mode fiber, the spectra of the long-wave (greater than ZDW) and the visible parts are very flat, as shown in Fig. 3, which is very advantageous for OCT applications.

4. THEORETICAL ANALYSIS

The FWM process participating in generating of a SC in a SMF pumped with a pulsed laser must satisfy the following equations [21]:

$$2h\omega_p = h\omega_a + h\omega_s, \tag{1}$$

$$\Delta\beta = \beta_a^j + \beta_s^k - 2\beta_p^l = 0, \tag{2}$$

$$\Delta\beta = \beta_a^j + \beta_s^k - \beta_p^l - \beta_p^m = 0, \tag{3}$$

where ω_p, ω_a, ω_s are the angular frequencies corresponding to the pump light, anti-Stokes light, and the Stokes light; and β_p^l, β_a^j, and β_s^k represent the propagation constants of the pump light, anti-Stokes light, and Stokes light in the l, j, and k modes, respectively.

For the FWM process, the energy conversion and phase-matching condition have to be satisfied simultaneously. When the two pump photons are in the same LP modes, the phase-matching condition is satisfied with a degenerate form in Eq. (2). While the two pump photons are in different modes, it must be satisfied with the form in Eq. (3), namely, the FWM process is IMFWM. For the IMFWM process participating for generating a SC in a SMF, the oscillating wavelengths of the Stokes light and the anti-Stokes light can be obtained by solving Eqs. (1)–(3).

First of all, the wavelength-dependent dispersion, effective refractive index, and propagation constants of the SMF (Corning SMF-28) were numerically simulated based on the finite difference eigen mode solver calculated by Mode Solution software. The dispersion, effective refractive index, and propagation constant of the SMF as a function of wavelength are shown in Fig. 5. The parameters used in the simulations are taken from the commercial SMF-28 such as the core radius of the fiber, $r = 4.1$ μm, and a core-cladding refractive index difference, $\Delta n = 0.0036$. The single-mode cutoff wavelength of the SMF is 1260 nm.

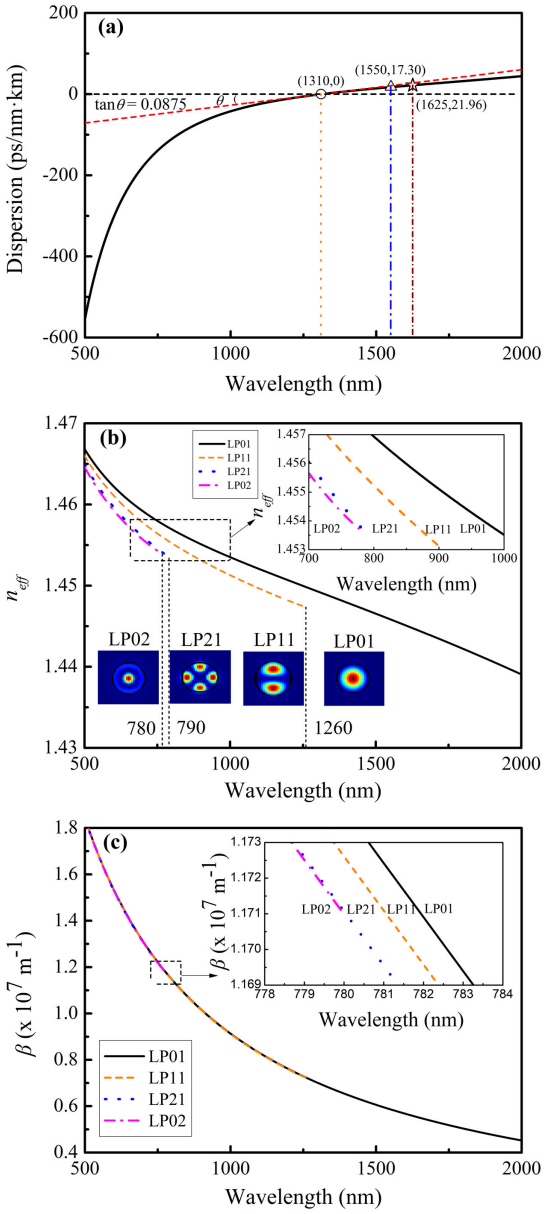

Fig. 5. (a) Dispersion, (b) effective refractive index, and (c) propagation constants as function of wavelength. Inset in (b) give some possible transverse modes participating in the IMFWM process.

From Fig. 5(a), we can see that the simulated ZDW is about 1310 nm, which is within the range from 1304 to 1324 nm measured for the SMF-28 fiber. The calculated zero-dispersion slope of 0.0875 ps/(nm^2 · km) is nearly equal to the measured value of 0.092 ps/(nm^2 · km). The dispersion values at 1550 and 1625 nm are 17.3 ps/(nm·km) and 27.96 ps/(nm·km), which are in good agreement with the measured data 18 ps/(nm·km) for 1550 nm and 22 ps/(nm·km) for 1625 nm. Therefore, the good agreement achieved between simulated wavelength-dependent dispersion of the SMF-28 fiber and experimentally measured data provides a solid foundation for the simulations. Figure 5(b) shows the calculated effective refractive index of four transverse modes propagating in the SMF as a function of the wavelength. The effective refractive index decreases with the wavelength for different transverse modes propagating in the SMF. However, the cutoff wavelengths of the LP11, LP21, and LP02 modes are 1260 nm, 790 nm, and 780 nm, respectively. For the pump laser working at 1030 nm, two transverse modes, LP01 and LP11, can transmit in the SMF-28 fiber. In the visible spectral region, high-order modes such as LP11, LP21, and LP02 are allowed for propagating in the SMF; therefore, more energy is expected to be extracted for generating SC in the visible region through the IMFWM process. Figure 5(c) depicts the propagation constant of four transverse modes as a function of the wavelength. It can be seen from Fig. 5(c) that the propagation constants of all four modes are pretty close with each other, which means only limited compensation can be provided for phase-matching conditions. Therefore, energy can be transferred to the short-wave sides by the IMFWM process, while the IMFWM process has a limited effect on generating new frequencies.

By applying wavelength-dependent dispersion, the effective refractive index, and propagation constants of the SMF-28 fiber theoretically obtained in Fig. 5, the IMFWM process in the SMF-28 fiber pumped with a 1030 nm pulse laser was studied theoretically by solving phase-matching equations Eqs. (1)–(3). Figure 6 shows the theoretically calculated phase-matching curves of IMFWM for different transverse mode combinations and two pump wavelengths.

As shown in Fig. 6(a), when the pump light is in a mixed mode, the anti-Stokes light in the LP11 mode with a wavelength of 1011 nm is obtained, and the corresponding Stokes light is in the LP01 mode with a wavelength of 1049 nm. The numerical results are well matched with the experimental data (1004/1058), as shown in Fig. 4. When a laser oscillating at 1004 nm as a pump light, there is a good agreement between the experimental data and the theoretical results for both cases above, as shown in Fig. 6(b). In fact, the structure of the fiber is difficult to maintain in the preparation process. There is a slight difference between the experimental results and the theoretical simulated results because the parameters of the fiber used for simulation are estimated from the fiber supplier and the thermal effect is not considered. However, the experimental results show that the transverse patterns of experimentally observed are consistent with the result of theoretical calculation, which proves the reliability of simulations and confirms that our explanation is reasonable. It is noted that the spectrum of the SC in the range of 600–800 nm is much flatter than that in the spectral range of 800–1000 nm, as shown in Fig. 3. For the IMFWM process, different transverse modes are required to propagate in the SMF. However, the transverse modes of the pump light, Stokes light, and anti-Stokes light participating in the SMF for generating a SC through the IMFWM process are limited by the different cutoff wavelengths of the transverse modes propagating in the SMF. From Fig. 5(b), we can see that only two transverse modes, LP01 and LP11, can propagate through the SMF-28 in the range of 800–1000 nm. In addition, for the SMF-28 under high peak power 1030 nm laser pumping, the anti-Stokes light generated through the IMFWM process in the range of 800–1000 nm oscillates in two transverse modes, while the corresponding Stokes light oscillates in the wavelength close to 1260 nm (the cutoff wavelength of the SMF supporting LP01 mode propagation). For the SMF, Stokes light can only

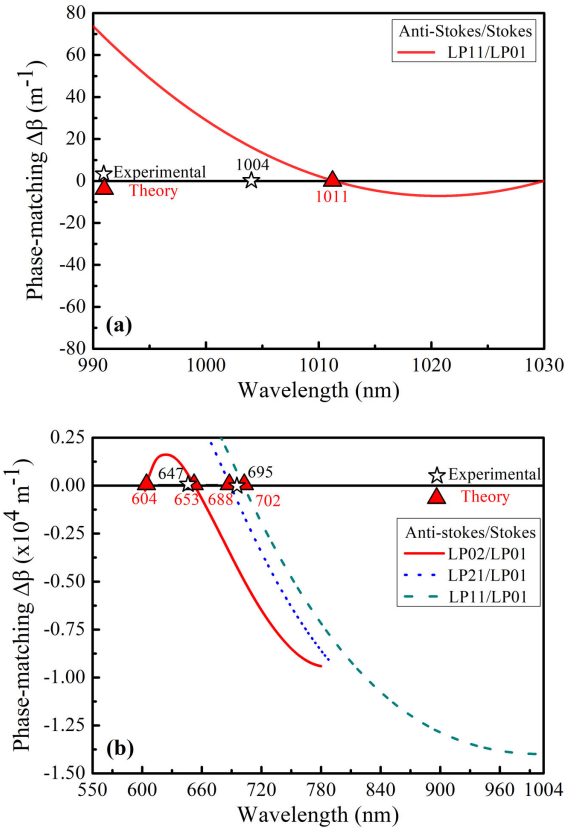

Fig. 6. Phase-matching curves of IMFWM for two pump wavelengths and mode configurations are shown in the legend. (a) Pump at 1030 nm, mixed mode configuration (LP01 + LP11) and (b) pump at 1004 nm, mixed mode configuration (LP01 + LP11, red line and blue dashed line), degenerate mode configuration (LP01 + LP01, cyan dotted line).

be transmitted in the LP01 mode. Conversely, in the spectral range of 600 to 800 nm, at least four transverse modes (LP01, LP11, LP21, and LP02) can propagate in the SMF. Therefore, high-order transverse modes such as LP02, LP11, and LP21 are generated in the SMF through the IMFWM process, which means more wavelengths able to generate in 600–800 nm. The spectral peaks become denser in this part and make the spectrum smoother. Furthermore, note the red line shown in Fig. 6(b). There are two anti-Stokes wavelengths in the visible region that satisfy the phase-matching condition. During the simulation, it is found that the same situation appears in a 10 nm bandwidth (from 1003 to 1013 nm). The simulated results are different from other phase-matching curves obtained in multi-mode fibers and few-mode fibers. The physical mechanism for such results obtained in the SMF is worth further investigation. Simultaneously generated two frequencies are helpful for transferring more energy from the pump light to the visible region and broadening the visible spectrum. Furthermore, the laser wavelengths generated in the SMF with the IMFWM effect are always within the visible spectral region during our simulation, and the new wavelengths generated are very close with each other. Thus, dense laser spectral peaks in 600–800 nm overlap each other, and make the peak structure relatively comparable. Therefore, the spectrum at 600–800 nm is flatter than that at 800–1000 nm in the SC.

5. CONCLUSION

A high-power, ultra-broadband supercontinuum light has been demonstrated in a SMF pumped with a nanosecond Yb : YAG/Cr^{4+} : YAG PQSML oscillating at 1030 nm. The spectral bandwidth of the SC is more than 1150 nm covering from 600 to 1750 nm, which is limited by the spectral range of the optical spectral analyzer. The maximum average output power of 181.8 mW is obtained at an input pump power of 880 mW, and the optical efficiency is as high as 20.6%. The net conversion efficiency is over 51.6% with respect to the pump power coupled into the fiber. The generation of ultra-broadband SC in the Yb : YAG/Cr^{4+}:YAG PQSML pumped SMF is attributed to the cascade SRS and IMFWM effects. Experimental results indicate that the IMFWM plays an important role to expand the spectrum of the SC to the visible region, which is in good agreement with the theoretical simulations. The visible part of the spectrum is very flat, which is very different from the results obtained in the few-mode fibers and multi-mode fibers. The high-power and ultra-broadband SC light working at 600–1750 nm provides more flexibility and sensitivity for potential application on OCT. This work provides an effective and simple method for developing highly efficient, high-power, SC light with ultra-broadband spectral range based on the traditional SMF and compact passively *Q*-switched lasers.

Funding. National Natural Science Foundation of China (61275143, 61475130); Program for New Century Excellent Talents in University (NCET-09-0669).

Disclosures. The authors declare no conflicts of interest.

REFERENCES

1. I. Hartl, X. D. Li, C. Chudoba, R. K. Ghanta, T. H. Ko, J. G. Fujimoto, J. K. Ranka, and R. S. Windeler, "Ultrahigh-resolution optical coherence tomography using continuum generation in an air-silica microstructure optical fiber," Opt. Lett. **26**, 608–610 (2001).
2. S. Dupont, Z. Qu, S. S. Kiwanuka, L. E. Hooper, J. C. Knight, S. R. Keiding, and C. F. Kaminski, "Ultra-high repetition rate absorption spectroscopy with low noise supercontinuum radiation generated in an all-normal dispersion fibre," Laser Phys. Lett. **11**, 075601 (2014).
3. J. Ye, J. L. Hall, S. T. Cundiff, and T. M. Fortier, "Carrier-envelope phase stabilization of femtosecond modelocked lasers and direct optical frequency synthesis," Science **288**, 635–639 (2000).
4. J. Swiderski, "High-power mid-infrared supercontinuum sources: Current status and future perspectives," Prog. Quantum Electron. **38**, 189–235 (2014).
5. J. W. Walewski, J. A. Filipa, C. L. Hagen, and S. T. Sanders, "Standard single-mode fibers as convenient means for the generation of ultrafast high-pulse-energy supercontinua," Appl. Phys. B **83**, 75–79 (2006).
6. R. S. Watt, C. F. Kaminski, and J. Hult, "Generation of supercontinuum radiation in conventional single-mode fibre and its application to broadband absorption spectroscopy," Appl. Phys. B **90**, 47–53 (2008).
7. J. C. Hernandez-Garcia, J. M. Estudillo-Ayala, O. Pottiez, R. Rojas-Laguna, R. I. Mata-Chavez, and A. Gonzalez-Garcia, "Generation of a spectrum with high flatness and high bandwidth in a short length of

telecom fiber using microchip laser," Opt. Commun. **292**, 126–130 (2013).
8. C. M. B. Cordeiro, W. J. Wadsworth, T. A. Birks, and P. St. J. Russell, "Octave supercontinuum generated in tapered conventional fibres by a nanosecond 1064 nm laser," in *Conference on Lasers and Electro-Optics/International Quantum Electronics Conference and Photonic Applications Systems Technologies*, California, USA (Optical Society of America, 2004), paper CThC2.
9. R. M. Tao, X. L. Wang, H. Xiao, P. Zhou, and J. Hou, "Near-IR supercontinuum generation based on a telecom single-mode fibre in an all-fibre format, and its power combining," Quantum Electron. **44**, 306–308 (2014).
10. X. M. Liu, L. R. Wang, D. Mao, and L. N. Duan, "Supercontinuum generation in standard single-mode fiber pumped by a nanosecond-pulse laser," Laser Phys. **22**, 227–231 (2012).
11. R. H. Stolen, J. E. Bjorkholm, and A. Ashkin, "Phase-matched three-wave mixing in silica fiber optical waveguides," Appl. Phys. Lett. **24**, 308–310 (1974).
12. J. Demas, P. Steinvurzel, B. Tai, L. Rishoj, Y. Chen, and S. Ramachandran, "Intermodal nonlinear mixing with Bessel beams in optical fiber," Optica **2**, 14–17 (2015).
13. S. Perret, G. Fanjoux, L. Bigot, J. Fatome, G. Millot, J. M. Dudley, and T. Sylvestre, "Supercontinuum generation by intermodal four-wave mixing in a step-index few-mode fibre," APL Photonics **4**, 022905 (2019).
14. P. Hamed, N. Elham, and M. Arash, "Detailed investigation of intermodal four-wave mixing in SMF-28: blue-red generation from green," Opt. Express **23**, 14487–14500 (2015).
15. P. Mondal, N. Bhatia, V. Mishra, R. Haldar, and S. K. Varshney, "Cascaded Raman and intermodal four-wave mixing in conventional non-zero dispersion-shifted fiber for versatile ultra-broadband continuum generation," J. Lightwave Technol. **36**, 2351–2357 (2018).
16. G. Lopez-Galmiche, Z. Sanjabi Eznaveh, M. A. Eftekhar, J. Antonio Lopez, L. G. Wright, F. Wise, D. Christodoulides, and R. Amezcua Correa, "Visible supercontinuum generation in a graded index multimode fiber pumped at 1064 nm," Opt. Lett. **41**, 2553–2556 (2016).
17. R. Dupiol, A. Bendahmane, K. Krupa, A. Tonello, M. Fabert, B. Kibler, T. Sylvestre, A. Barthelemy, V. Couderc, S. Wabnitz, and G. Millot, "Far-detuned cascaded intermodal four-wave mixing in a multimode fiber," Opt. Lett. **42**, 1293–1296 (2017).
18. J. Dong, A. Shirakawa, and K. I. Ueda, "Sub-nanosecond passively Q-switched Yb : YAG/Cr^{4+}: YAG sandwiched microchip laser," Appl. Phys. B **85**, 513–518 (2006).
19. J. Dong, Y. Y. Ren, and H. H. Cheng, ">1 MW peak power, an efficient Yb:YAG/Cr^{4+}:YAG composite crystal passively Q-switched laser," Laser Phys. **24**, 055801 (2014).
20. M. E. Fermann, "Single-mode excitation of multimode fibers with ultrashort pulses," Opt. Lett. **23**, 52–54 (1998).
21. G. Agrawal, "Chapter 8–stimulated Raman scattering," in *Nonlinear Fiber Optics*, 5th ed., (Academic, 2013), pp. 295–352.
22. Y. Kodama and A. Hasegawa, "Nonlinear pulse-propagation in a monomode dielectric guide," IEEE J. Quantum Electron. **23**, 510–524 (1987).
23. F. M. Mitschke and L. F. Mollenauer, "Discovery of the soliton self-frequency shift," Opt. Lett. **11**, 659–661 (1986).
24. J. P. Gordon, "Theory of the soliton self-frequency shift," Opt. Lett. **11**, 662–664 (1986).
25. J. C. Travers, "Blue extension of optical fibre supercontinuum generation," J. Opt. **12**, 113001 (2010).
26. P. K. A. Wai, C. R. Menyuk, Y. C. Lee, and H. Chen, "Nonlinear pulse propagation in the neighborhood of the zero dispersion wavelength of single-mode fibers," in *International Quantum Electronics Conference*, California, USA (Optical Society of America, 1986), paper WGG19.
27. N. Akhmediev and M. Karlsson, "Cherenkov radiation emitted by solitons in optical fibers," Phys. Rev. A **51**, 2602–2607 (1995).
28. F. Biancalana, D. V. Skryabin, and A. V. Yulin, "Theory of the soliton self-frequency shift compensation by the resonant radiation in photonic crystal fibers," Phys. Rev. E **70**, 016615 (2004).
29. K. Yin, B. Zhang, W. Yang, H. Chen, and J. Hou, "Over an octave cascaded Raman scattering in short highly germanium-doped silica fiber," Opt. Express **21**, 15987–15997 (2013).